



# 1 GPS displacement dataset for study of elastic surface mass 2 variations

3

4 Athina Peidou<sup>1</sup>, Donald Argus<sup>1</sup>, Felix Landerer<sup>1</sup>, David Wiese<sup>1</sup> and Matthias Ellmer<sup>1</sup>  
5 Jet Propulsion Laboratory, California Institute of Technology, Pasadena, CA, USA, 2023

6

7 *Correspondence to:* Athina Peidou ([athina.peidou@jpl.nasa.gov](mailto:athina.peidou@jpl.nasa.gov))

8 © 2023. California Institute of Technology. Government sponsorship acknowledged.

## 9 Abstract

10

11 Quantification of uncertainty in surface mass change signals derived from GPS measurements poses  
12 challenges, especially when dealing with large data sets with continental or global coverage. We present a  
13 new GPS station displacement data set that reflect surface mass load signals and their uncertainties. We  
14 assess the structure and quantify the uncertainty of vertical land displacement derived from 3045 GPS  
15 stations distributed across the continental US. Monthly means of daily positions are available for 15  
16 years. We list the required corrections to isolate surface mass signals in GPS estimates and screen the data  
17 using GRACE(-FO) as external validation. Evaluation of GPS timeseries is a critical step, which  
18 identifies a) corrections that were missed; b) sites that contain non-elastic signals (e.g., close to aquifers);  
19 and c) sites affected by background modelling errors (e.g., errors in the glacial isostatic model). Finally,  
20 we quantify uncertainty of GPS vertical land displacement (VLD) estimates through stochastic modeling  
21 and quantification of spatially correlated errors. Our aim is to assign weights to GPS estimates of VLD,  
22 which will be used in a joint solution with GRACE(-FO). We prescribe white, colored and spatially  
23 correlated noise. To quantify spatially correlated noise, we build on the common mode imaging approach  
24 adding a geophysical constraint (i.e., surface hydrology) to derive an error estimate for the surface mass  
25 signal. We study the uncertainty derived using each technique and find that three techniques exhibit an  
26 average noise level between 2-3 mm: white noise, flicker noise, and RMS of residuals about a seasonality  
27 and trend fit. Prescribing random walk noise increases the error level such that half of the stations have  
28 noise > 4 mm, which is systematic with the noise level derived through modeling of spatial correlated  
29 noise. The new data set is suitable for use in a future joint solution with GRACE(-FO)-like observations.

30

31 **Keywords:** GPS uncertainty | vertical land displacement | GRACE-FO | surface mass change

32

## 33 1. Introduction

34

35 For more than two decades, the Gravity Recovery and Climate Experiment (GRACE) space gravity  
36 mission and its nearly identical successor mission, GRACE-Follow on (GRACE-FO), have provided  
37 mass change estimates through tracking the time-variable part of the Earth's gravity field (Landerer et al.,  
38 2020). Mass change products are typically given on a monthly basis and have been used to study a variety  
39 of critical climate-related factors (Tapley et al., 2019), such as sea level rise (Frederikse et al., 2020); ice



40 mass change (Velicogna et al., 2020); prolonged drought periods (Thomas et al., 2014) and regional flood  
41 potentials (Reager et al., 2014). The measurement geometry of GRACE(-FO) limits the study of  
42 geophysical processes to spatial scales of ~300 km and larger, for monthly timespans. Recent community  
43 reports (Pail et al., 2015, Wiese et al., 2022) have highlighted the utility and need of mass change  
44 observations at improved spatial resolutions to address a number of science and applications objectives.  
45 Examples include closure of the terrestrial water budget for small to medium sized river basins, and  
46 separation of surface mass balance from ice dynamic processes at the scale of individual outlet glacier  
47 systems.

48 The spatial resolution of gravity maps derived from satellite measurements is limited by sampling at  
49 altitude. Fusion with external geodetic data sources, however, can improve spatial resolution over what  
50 can be achieved only with satellite gravimetry. GPS position timeseries have been used widely to study  
51 the elastic response of Earth's surface to mass loading (e.g., Argus et al., 2017; Fu and Freymueller,  
52 2012) and can provide information at short wavelengths (~100km) (Argus et al., 2021). Solid Earth  
53 responds elastically to changes in the surface load of water, snow, ice, and atmosphere. When the Earth's  
54 surface is loaded with mass (e.g., snow and water) it subsides; and when mass loads are removed the  
55 surface rises. Thus, the Earth's response follows the water cycles such that: precipitation and snow  
56 accumulation subside the surface and snow melt, evaporation and water run off allow the Earth's surface  
57 to bounce back (uplift). Focus is typically placed on the radial direction (vertical), due to the rapid  
58 decrease of vertical land displacement (VLD) with the distance from a surface load (Argus et al., 2017),  
59 which leads to high fidelity estimates in the space domain. Note that across certain geological formations  
60 such as aquifers, subduction zones and regions with volcanic activity surface loading is mixed with other  
61 solid Earth/geophysical processes making it difficult to isolate the elastic component. Therefore, GPS  
62 sites located at the vicinity of such formations are omitted from further analyses.

63 GPS VLDs (i.e., displacement between two epochs) have many different signals embedded in them; i.e.,  
64 those related to atmospheric and oceanic loading, solid Earth phenomena such as tectonics, glacial  
65 isostatic adjustment (GIA), and others related to surface mass changes. With the proper treatment (see  
66 Sec.2) GPS stations can capture local surface mass changes. We are interested in isolating the signals that  
67 reflect the Earth's elastic response to mass variations, thus we apply a set of corrections to GPS VLD  
68 estimates, and then we screen the data for outliers or potential errors. The data screening process checks  
69 for consistency between GPS and GRACE(-FO) VLD estimates (similar analysis has been performed by  
70 Yin et al., 2020; Blewitt et al., 2001; van Dam et al., 2001; Becker and Bevis, 2004; Davis, 2004;  
71 Tregoning et al., 2009; Tsai, 2011 and Chew et al., 2014) and identifies outliers that statistical tests fail to  
72 pick up (He et al., 2018).

73 The last step is to estimate uncertainty in the screened data set. Since our purpose is to isolate surface  
74 mass load signals, we define *error* as any VLD signal that does not reflect an elastic surface mass load.  
75 The reported uncertainty of a measurement reflects the sum of all error sources to the measurement, and is  
76 the final product of this study. Error correlation (temporal and spatial) and the deficiency of stochastic  
77 noise models to describe the error realistically are the main challenges in this uncertainty quantification  
78 task.

79 Error sources include errors driven by satellite antenna phase centre offsets (Santamaria-Gomez et al.,  
80 2012); atmospheric pressure models (Kumar et al., 2020); non-tidal ocean loading (Jiang et al., 2013);  
81 satellite orbits (Ray et al., 2008; Amiri-Simkooei, 2013); earth orientation parameters (Rodriguez-Solano  
82 et al., 2014); and tectonic trends and post-seismic relaxation after earthquake activity (Ji and Herring,  
83 2013; Crowell et al., 2016).



84 Most of these errors are also spatially coherent, and their sum is usually referred to as common-mode  
85 noise (CMN) (Kreemer and Blewitt; 2021). Mitigation of CMN is usually done by means of spatial  
86 filtering (Wdowinski et al. 1997), a technique that needs to be applied with caution, due to the  
87 assumptions made when applying a spatial filter (see e.g., Williams, 2004; Tian and Shen 2016).  
88 Recent developments of spatial filtering algorithms include principal component analysis (PCA) or  
89 independent component analysis (ICA). PCA decomposes residual time-series (relative to a deterministic  
90 model) into various principal/independent components based on their variance and identifies the  
91 components that reflect CMN (Serpelloni et al., 2013; Li and Shen, 2018). ICA is different than PCA in  
92 that it finds the maximum independence of the components instead of minimum correlation (Milliner et  
93 al., 2019; Liu et al., 2015). One of the main limitations of PCA/ICA is their susceptibility to dismiss  
94 CMN reflected in a relatively small number of stations. Therefore, in many occasions a subset of stations  
95 is studied independently (Wu et al., 2019).  
96 Considering the increased number of GPS stations and the limitations posed by the existing  
97 methodologies, Kreemer and Blewitt (2021) developed a robust methodology to estimate the common  
98 spatial components of GPS residuals (i.e., the remaining signals of a time-series after subtraction of a  
99 deterministic model). The so-called common mode component (CMC) imaging technique quantifies the  
100 spatial correlation of the residuals (position or VLD time-series anomaly with respect to a deterministic  
101 model) of unequal-length time-series using information from neighbor stations. It is important to note that  
102 CMC reflects both spatially correlated noise and spatially correlated signals, including elastic  
103 displacements, that a deterministic model fails to describe.  
104 Spectral analysis of the residuals (with respect to a deterministic model, see Eq.2) is an alternative way to  
105 estimate the noise level of VLD series for each GPS station. The spectrum of the residuals can be  
106 approximated by white or colored noise (flicker, random walk, power law approximation, generalized  
107 gauss markov etc.), or by a combination of white and colored noise (Williams et al., 2004; Bos et al.,  
108 2008; Klos et al., 2014). A summary of the different noise models and their power distribution can be  
109 found in He et al. (2018). Several standard GPS time series analysis packages are available to perform  
110 such an analysis, e.g., CATS (Williams, 2008) and Hector (Bos et al. 2013). Various studies in the past  
111 suggested that the residuals are better described by a combination of white and flicker noise (see e.g.,  
112 Klos et al., 2014; Argus et al., 2017), with the latter contributing the most (Argus and Peltier, 2010).  
113 Recently, Argus et al. (2022), showed that the longer the timeseries the more the spectrum of GPS  
114 residuals converges with the noise model of random walk.  
115  
116 In this contribution, we outline a comprehensive framework for processing large data sets (continental  
117 and/or global) of GPS VLD timeseries, to derive VLD estimates that only reflect surface mass signals, for  
118 use in a joint inversion with GRACE(-FO) measurements. Originally, we layout the corrections required  
119 to capture local surface mass changes (Section 2.1). Our interest is to make the process as automated as  
120 possible, thus we set a number of evaluation metrics to detect outliers among all candidate (for the joint  
121 inversion) sites. Stations flagged as outliers are further evaluated for extra corrections (e.g., offsets; poor  
122 site maintenance etc.). Finally, we assign weights to each GPS VLD record. We test the most popular  
123 methodologies to quantify the error, considering time-correlation, spatial-correlation and/or white noise  
124 (Section 3). Note that for spatially correlated noise the commonly used PCA/ICA is not as applicable to  
125 our use case, because our data set extends over very large spatial areas (continental). CMC imaging  
126 (Kreemer and Blewitt; 2020) fits our needs better. We overcome CMC's limitation of include spatially  
127 correlated hydrology signals in the error estimate by deriving surface loading signals from a hydrology



128 model and removing them. The final product is a new data set with GPS VLD estimates that reflect elastic  
129 mass variations and their uncertainties.

## 130 **2. GPS data processing and screening**

131

### 132 2.1 Isolating surface mass loading fingerprint from GPS VLD

133

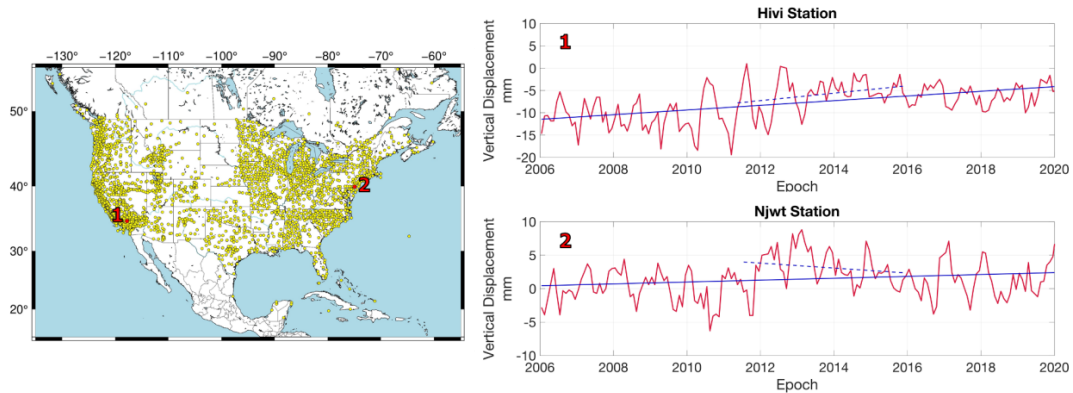
134 The 3054 GPS position time-series used in this study are a product of Jet Propulsion Laboratory (JPL)  
135 (Bertiger et al., 2020) and Nevada Geodetic Laboratory reprocessed GPS solutions (Blewitt et al., 2018).  
136 GPS satellite orbits, clocks, and core site positions are estimated consistently using the latest techniques  
137 and GipsyX software (Bertiger et al., 2020). Displacement signals driven by solid earth, oceanic and pole  
138 tides are corrected according to International Earth Rotation Service (IERS) standards.

139 We process the GPS series similar to Argus et al. (2017; 2022), that is, we correct for atmospheric loading  
140 signals using the ECMWF weather model (Simmons et al., 2007) and for GIA, using the ICE-6G\_D  
141 model (Peltier et al., 2018). GIA modelling errors affect GPS and GRACE(-FO) VLD predictions in  
142 opposite sense. Overestimation of GIA translates to subsidence when we correct GPS. The same  
143 overestimation predicts too much mass gain and shows as water loss when we correct GRACE(-FO),  
144 which eventually translates to land uplift. The same analogy applies to underestimation of GIA, which is  
145 mapped as uplift on GPS and as subsidence on GRACE(-FO) VLD predictions.

146 Estimates prior to or after a significant earthquake event, or biased by a significant post-seismic transient  
147 are discarded. Stations with non-elastic response (e.g., porous) located at aquifers, volcanically active  
148 regions and oil extraction sites are also removed from the data record (see Argus et al. (2017) for details).  
149 An interseismic strain accumulation correction across the Cascadia is also applied (Argus et al., 2021).  
150 The model (Li et al. 2018) consists of both elastic and viscous components (2/3 elastic and 1/3 viscous).  
151 All estimates are given in the International Terrestrial Reference Frame 2014 (Altamimi et al., 2016).  
152 Finally, we solve for and remove an offset (Argus et al., 2010) if an estimated offset is greater than 8 mm  
153 in the radial direction. In most cases, estimating the offset reduces the root mean square dispersion (in  
154 mm) of the position estimates about a fit of the position, velocity and sinusoid with an annual frequency,  
155 by more than 5 percent. Daily solutions are averaged into monthly means, and are available for different  
156 durations over a span of fifteen years starting from 2006.

157 To compare GPS with GRACE(-FO) VLD estimates we reference all VLD data to the epoch with the  
158 most GPS site records, which is September 2012. This process results in an 11% loss of stations (i.e., no  
159 available measurement on 09/2012). Similar to Yin et al. (2020), detrended monthly estimates of each  
160 station that are larger than  $3\sigma$  relative to the mean of the time-series are considered outliers and removed  
161 from the data set. Statistical outliers comprise ~0.5% of the records.

162 2705 (or 88.8%) of GPS stations remain after the choice of reference epoch, the  $3\sigma$  test and the removal  
163 of sites with non-elastic loading response. The distribution of sites is denser along the East and West  
164 coasts, and fairly sparse in the central-north US (Fig.1). Series of two arbitrary stations (hivi and njwt)  
165 located at the West and East coast respectively, are shown in Fig. 1. The response of the Earth on the  
166 extensive drought period in California between 2011.5-2015.5 is captured in the uplift trend mapped by  
167 hivi station (Fig.1, top right panel; dashed blue line).



168  
 169 Figure 1: Left panel) Map of study area. GPS stations are shown in yellow; Right panel) Vertical  
 170 displacement timeseries of two random stations (red line). Solid blue line denotes the overall trend of the  
 171 timeseries and dashed blue line the trend between (2011.5-2015.5). Note the significant uplift of the hivi  
 172 station located in southern California.

173  
 174 2.2 External validation data sets - Time-variable gravity field  
 175

176 We employ GRACE(-FO) mascon solutions developed at the Jet Propulsion Laboratory that resolve mass  
 177 changes using 3-degree spherical cap basis functions (Wiese et al., 2016; Watkins et al., 2015) as a  
 178 validation tool for the GPS data. The effect of postglacial rebound is removed from GRACE(-FO)  
 179 products using ICE-6G\_D model estimates (Peltier et al., 2017). The geocentre motion (degree 1)  
 180 coefficient is replaced with the estimated coefficient from Sun et al. (2016), using TN-13. The Earth's  
 181 oblateness coefficient ( $C_{20}$ ) is replaced by an estimate derived from Satellite Laser Ranging observations  
 182 for all months (Loomis et al., 2019), as is the  $C_{30}$  coefficient for all months after August 2016, due to  
 183 only having a single functioning accelerometer. GPS position timeseries do not include the linear trend of  
 184 the geocentre motion (i.e., the linear trend of the ITRF14 frame is approximately zero, Altamimi et al.  
 185 (2014)), as opposed to GRACE(-FO), thus we remove it from GRACE(-FO). The annual signal of the  
 186 geocentre (as realized by ITRF14) projected on the up component in north America can explain up to  
 187 20% of the GPS VLD signal.

188 GRACE(-FO) VLD monthly estimates are derived as follows (e.g., Davis et al., 2004):  
 189

$$U(\phi, \lambda) = a \sum_{l,m} \left( \frac{h_l^E}{1 + k_l^E} \right) P_{lm}(\sin\lambda) \times [C_{lm} \cos m\phi + S_{lm} \sin m\phi] \quad (1)$$

190  
 191 Where,  $U$  is the estimate of vertical displacement,  $a$  denotes the Earth's radius,  $\phi, \lambda$  denote the latitude  
 192 and longitude, respectively; are the associated Legendre polynomials, and are the elastic and vertical Love  
 193 numbers (PREM; Wang et al., 2012), respectively, and  $C$  and  $S$  are the spherical harmonic coefficients  
 194 derived from GRACE(-FO) monthly solutions with respect to degree  $l$  and order  $m$ . Similar to GPS, we  
 195 subtract September 2012 values from the rest of the series for a common reference basis.  
 196



197 2.3 Screening metrics

198

199 GPS VLD estimates are evaluated against the ones derived from GRACE(-FO), to assist in identifying  
200 outliers or further corrections that may be needed. We employ a number of different metrics to evaluate  
201 the agreement between the two data sets, and to determine whether to include it in the joint solution or  
202 not. Similar to Yin et al. (2020) we quantify correlation and variance reduction between GPS and  
203 GRACE(-FO) VLDs. The structure of surface mass periodic signals (e.g., annual cycles, trends) as picked  
204 up by the two measurement platforms, also entails critical information regarding mismodelled offsets, and  
205 is evaluated as well.

206 This process flags sites that need correction and corroborates joint inversion's hypothesis (Argus et al.,  
207 2021), that a basic level of agreement is needed for the GPS data to be used to infer surface mass change.

208

209

210 *Correlation*

211

212 First, we specify the level of agreement between the data sets by estimating the Pearson correlation  
213 coefficient between GPS & GRACE(-FO) VLD timeseries. On average the correlation is 62%, but  
214 stations located on the West coast exhibit an agreement higher than 80%, which in most cases is driven by  
215 the larger annual signal amplitude. A more detailed look into the correlation metric is performed to  
216 evaluate the agreement of GPS/GRACE(-FO) in retrieving the seasonal cycle amplitude in different  
217 watersheds. We fit and remove a deterministic model  $y(t)$ :

218

$$y = a + bt + A + B\cos(2\pi t), \quad (2)$$

219

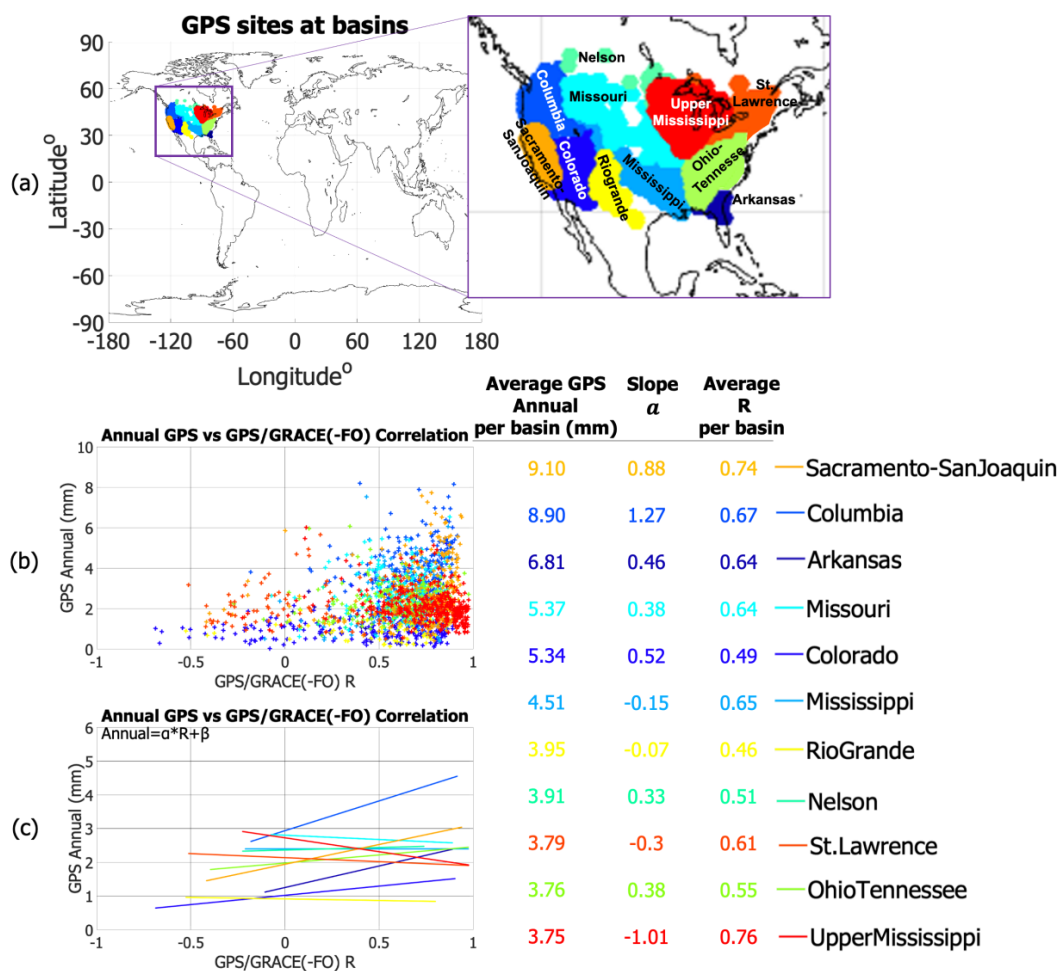
220 with  $a$  being the intercept;  $b$  being the trend and  $A$  and  $B$  being the amplitude and phase of a periodic  
221 function with annual frequency.

222

223 We classify stations in watersheds and plot the GPS-GRACE(-FO) correlation coefficient ( $R$ ) of each  
224 station in different watershed against the amplitude of annual signals (Fig. 2b). To quantify the  
225 relationship between magnitude of the annual cycle and correlation between the two data sets we fit a  
226 linear function between the magnitude of the annual signals and the GPS-GRACE(-FO) VLD correlations  
227 for each watershed, separately. A steep slope ( $\alpha$ ) of the fit ( $\alpha > 0.5$ ) indicates an agreement between the  
228 two data sets, which depends on the magnitude of the annual cycle. This relationship breaks when stations  
229 of a basin exhibit smaller annual cycles. We discuss an interesting case in Supplements, where stations  
230 located in the St. Lawrence basin demonstrate a negative trend  $\alpha = -1.26$ . The disagreement is even  
231 more pronounced while assessing the second metric (i.e., trends). Both metrics, when taken together,  
232 helped us identify the source problem (i.e., unlogged offset) and take corrective actions (see Supplements  
233 for more details). Note that for Figs. 2 and 3 the corrected data were used.

234

235



236  
 237  
 238 Figure 2: a) GPS sites clusters at watersheds in the US. Each watershed has a different color; b)  
 239 Magnitude of annual GPS VLD cycles derived with respect to GPS-GRACE(-FO) correlation; c) Linear  
 240 fit between magnitude of the annual GPS VLD cycles and GPS-GRACE(-FO) correlation.

241  
 242 *Trends*

243  
 244 In order to study the agreement between GPS/GRACE(-FO) in more detail, we split the timeseries of each  
 245 station into non-overlapping intervals of 36 months, and fit Eq.2 for each station during each time-  
 246 window. Different time-lengths of the GPS series may lead to misinterpretation of the geophysical  
 247 content. For example, a station that has records only for the first 13 months out of the total of 36 months  
 248 window may reflect different fit constituents compared to a neighbor station with full records, if the  
 249 actual behavior of Earth's response changes during the 36-months window. Although in our data set this  
 250 case is fairly rare, we proceed with deriving the rate (slope) and the annual cycles only for stations that



251 have records for at least 28 out of the 36 months. As expected, GPS rates feature higher spatial variability  
252 than GRACE(-FO). However, both platforms capture large-scale quasi-periodic variations every 3 years  
253 (Fig. 3), an agreement that is noteworthy. The effect of this metric to detect outliers is pronounced when  
254 the two platforms show flipped trends.

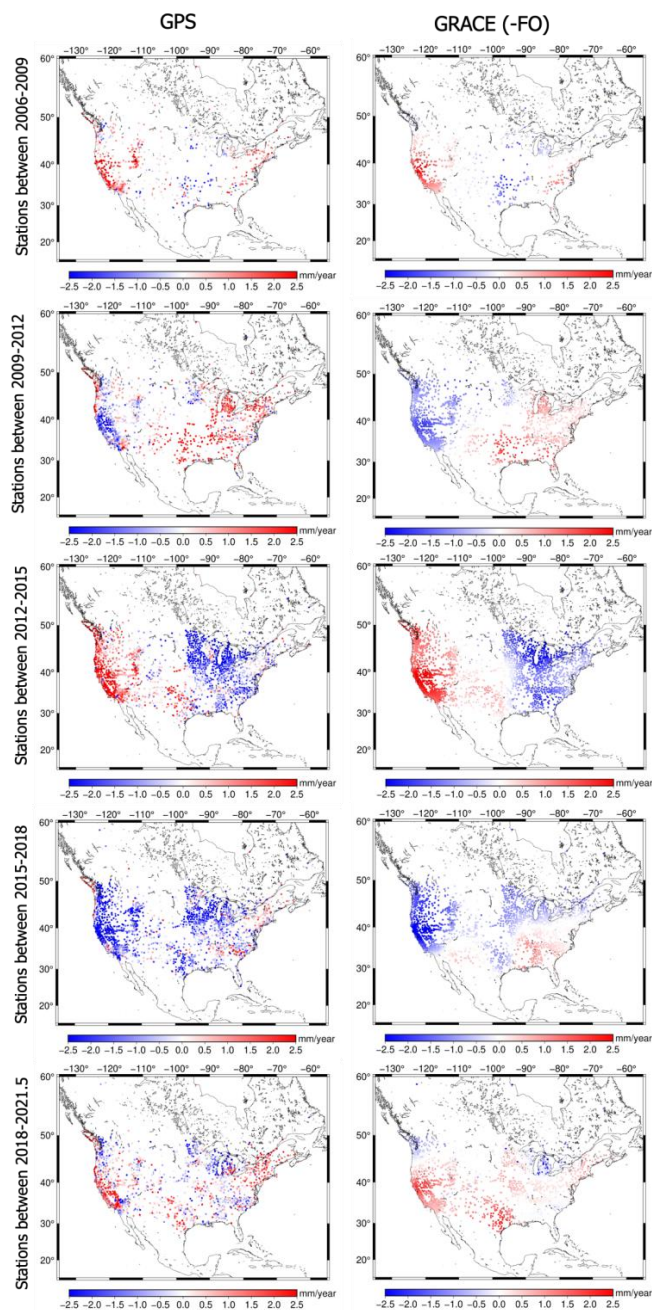
255

256 Regions with pronounced trend disagreement:

- 257 • Great Lakes area (St. Lawrence watershed). The trend during 2015-2018 was flipped between  
258 GPS and GRACE(-FO). We discovered a missed offset in the series occurring in April 2016, and  
259 corrected for it, which the agreement in the trend (see Supplements).
- 260 • Cascadia region (northwest coast). The disagreement is evident in maps spanning 2009-2012,  
261 2015-2018 and 2018-2021.5. GPS sites record a large surface uplift, which over the course of 15  
262 years sums to 60 mm in sites located in Vancouver Island. GRACE(-FO) does not capture any  
263 such behavior. We attribute this disagreement partly on 1) GIA modeling error which manifests  
264 oppositely on two platforms. ICE6G\_D predicts too much subsidence, thus when we correct GPS  
265 we find too much uplift and when we correct GRACE(-FO) we find too much water gain which  
266 predicts too much subsidence; and partly on 2) the interseismic strain accumulation correction  
267 applied in the GPS data set over this area (Argus et al., 2021). The sites have been flagged and are  
268 not going to be used in the joint inversion.
- 269 • San Andreas Fault (Southern California). Sites located in a vicinity of the Parkfield segment of  
270 the fault (Carrizon plain), exhibit consistent disagreement in the trend. More investigation is  
271 required to understand the mechanism that the fault presents on GPS/GRACE(-FO) VLD  
272 estimates. The disagreement is also seen in Argus et al. (2022, Fig. S12). The sites have been  
273 flagged and are not going to be used in the joint inversion.

274





275  
276  
277

Figure 3: Rates of vertical displacements derived by GPS and GRACE. The rates are calculated every 36-months (3 years) between 2006-2021.

278  
279



280 *Variance Reduction*

281

282 Similarity in both amplitude and phase between two quantities is quantified via the variance attenuation  
283 factor (Gaspar and Wunsch, 1989; Fukumori et al., 2015):

284

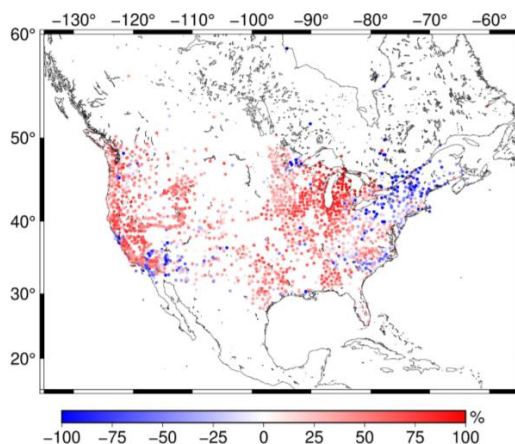
$$var_{red} = \left( 1 - \frac{var(GPS - GRACE(-FO))}{var(GPS)} \right) \times 100 \quad (3)$$

285

286 The higher the agreement in phase and amplitude between GPS and GRACE(-FO), the closer the metric  
287 gets to 100%.  $var_{red}$  may also be negative when the differences in amplitude and/or phase are large.

288 Overall, GPS and GRACE(-FO) are consistent when  $var_{red}$  exceeds 50%. The areas of main  
289 disagreement are near coasts, especially along the Atlantic Ocean. This inconsistency can be partly  
290 explained by modeling errors of the non-tidal oceanic and atmospheric loading model (e.g., Klos et al.,  
291 2021; van Dam et al., 2007). Additionally, agreement is poor for sites located in the vicinity of the  
292 Parkfield segment (specific regions across the fault perform poorly), which is consistent with the  
293 disagreement shown in Fig. 3.

294



295

296 Figure 4: Variance reduction between GPS and GRACE(-FO) VLD

297

298 We also compared the amplitudes of GPS and GRACE(-FO) VLD periodic cycles. This analysis was not  
299 informative for the presence of outliers or errors.

300

301 Overall, the screening process not only assisted in outlier detection, but it also allowed for a deeper look  
302 into the structure of VLD periodic signals. We identified the need for antenna offset corrections (in the  
303 case of Great Lakes); removed sites affected by GIA and interseismic modeling errors; and sites located at  
304 the Parkfield segment of San Andreas Fault.

305

306

307



### 308 3. Uncertainty Quantification

309

310 With the updated data set we are now ready to proceed with the uncertainty quantification of the GPS  
311 VLD timeseries. We apply different error characterization schemes consisting of a root sum square of a  
312 random error, white noise error, power law noise error (flicker noise and random walk) and spatially  
313 coherent error.

314

#### 315 3.1 Methods

316

##### 317 *Root Mean Square Error*

318

319 Residuals  $r$  of a series with respect to a deterministic model (Eq. 2) are often used as a first  
320 approximation of noise in VLD series (e.g., Bos et al., 2013; Michel et al., 2021). Practically,  $r$  shows  
321 how well a deterministic model can describe the original time-series. Therefore, the root mean square  
322 (rms) of  $r$  can give a first approximation of the noise floor of each station.

323

##### 324 *Spectral Analysis, White, Flicker and Random Walk Noise*

325

326 Power distribution of residuals and its agreement with noise models, is another popular way to quantify  
327 uncertainty of GPS time-series (e.g., Klos et al., 2019; Argus et al., 2022). Typically, GPS series are  
328 evaluated for white, flicker and random walk noise, or combination of them. The Hector software (Bos et  
329 al., 2013) is used to estimate full noise covariance information by means of a maximum likelihood  
330 estimator. The covariance matrix  $C$  from a combination of white and power law (i.e., flicker and random  
331 walk) noise is given as:

332

$$C = a \times \mathbf{I} + b \times \mathbf{J} \quad \text{Eq. 4}$$

333

334 Where  $a$  is the amplitude of white noise,  $\mathbf{I}$  is the identity matrix of size  $N$  (number of samples/epochs in  
335 the series),  $b$  is the amplitude and  $\mathbf{J}$  the covariance matrix of power law noise.  $\mathbf{J}$  matrix is a full  
336 covariance matrix that describes the time-correlated error (as the data record length increases, the  
337 displacement uncertainty changes (Bos et al., 2008 Eqs. 8-11)). The optimal selection of the noise models  
338 is done via two optimality criteria, namely the Akaike Information Criterion (Akaike, 1974) and the  
339 Bayesian Criterion (Schwarz, 1978).

340

341 In this study, we consider three cases:

342

a) White Noise (WN)

343

b) Combination of WN and Flicker Noise (WN+FN)

344

c) Combination of WN, FN and Random Walk Noise (WN+FN+RW)

345

We take the root-sum-squares of the noise magnitudes as our noise floor. For example, for the case of

346

WN+FN noise, noise is derived as  $\sigma = \pm\sqrt{\sigma_{WN}^2 + \sigma_{FN}^2}$ . Our data are sampled on a monthly basis, thus



347  $\sigma_{FN}$  needs to be scaled appropriately, i.e.,  $\sigma_{FN} = \sigma_{PL} \left(\frac{1}{12}\right)^{-\frac{k}{4}}$ , where,  $\sigma_{PL}$  is the uncertainty of power-law  
 348 (PL) and  $k$  the spectral index, outputted from Hector (more information on power-law noise estimation  
 349 can be found in Bos et al., 2008, and Williams, 2003).

350

351 *Common Mode Noise*

352

353 The Common Mode Component (CMC) is derived following the processing scheme suggested by  
 354 Kreemer and Blewitt (2021), which can be summarized as:

355

- 356 1) Input GPS VLD time-series (referenced to Sep 2012) for  $j$  stations ( $l_j$ )
- 357 2) Derive each station's residuals by removing the deterministic part of the series ( $l_j(t) - y_j(t)$ )
- 358 3) Quantify the correlation coefficient  $r_{MAD}$  using robust statistics.  $r_{MAD}$  is defined as:

$$r_{MAD} = \frac{MAD^2(u) - MAD^2(v)}{MAD^2(u) + MAD^2(v)} \quad \text{Eq. 5}$$

359

360 where MAD is the median absolute value and  $u$  and  $v$  are derived as:

$$u = \frac{p - \text{median}(p)}{\sqrt{2}MAD(p)} + \frac{q - \text{median}(q)}{\sqrt{2}MAD(q)} \quad \text{Eq. 6}$$

$$v = \frac{p - \text{median}(p)}{\sqrt{2}MAD(p)} - \frac{q - \text{median}(q)}{\sqrt{2}MAD(q)} \quad \text{Eq. 7}$$

361

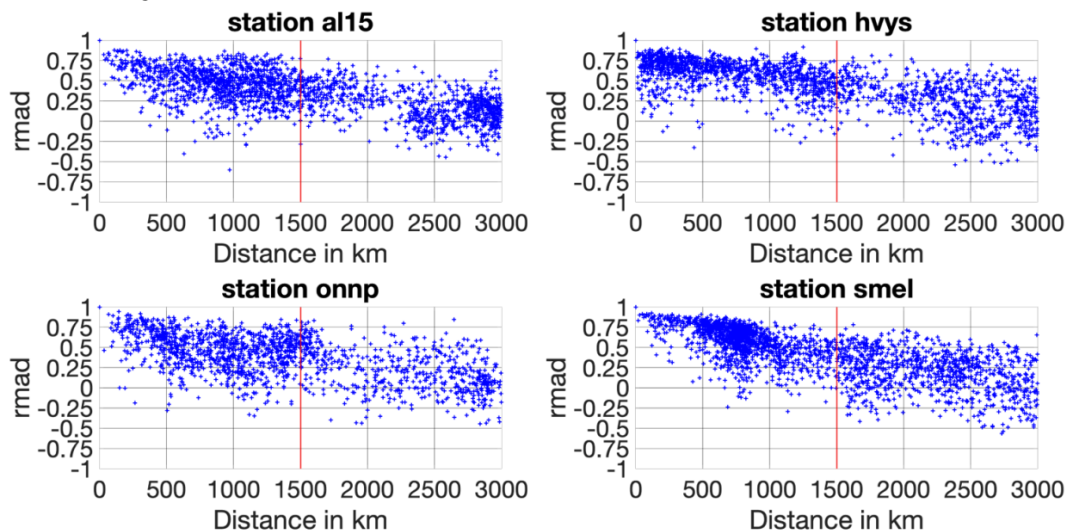
362 with  $p$  and  $q$  being the residual series of the reference station and the neighbor station, respectively.  
 363 For each station there are  $j - 1$  correlation coefficients  $r_{MAD}$ . In order to decide the cut-off distance  
 364 that a neighbor station will be considered in the analysis we plot  $r_{MAD}$  coefficient against its distance  
 365 from the reference station (Fig. 5). Based on results from all stations we decide to set a cut-off at 1500  
 366 km, slightly higher than the 1350 km suggested by Kreemer and Blewitt (2021). The 1500 km cut-off  
 367 allows us to separate stations between east and west coast, as spatially coherent signals at stations  
 368 located across the continent are negligible.

- 369 4) Derive the median slope estimator  $ccs$  using Theil-Sen median trend.

- 370 5) Derive the zero-distance intercept  $cci_j$  for each station as  $\text{median}(r_{MAD} - ccs * d)$ , with  $d$  being the  
 371 distance between the station of reference and the neighbor station (maximum  $d = 1500$  km).



- 372 6) Construct CMC: Calculate the cumulative ( $c_j$ ) and percentile ( $p_j$ ) weights for each station and then  
373 find the weighted median that corresponds to  $p_j = 50\%$ . This weighted median represents the CMC of  
374 the station (Fig. 6).



375 Figure 5: coefficient of four random stations with the rest of the station sample, plotted against the  
376 distance of the reference station with the rest of the stations. Each cross resembles the of the reference  
377 station with a station located at distance  $d$ .  
378  
379

380 CMC is limited in providing a realistic error approximation, in that the technique cannot isolate spatially  
381 correlated noise from signal (e.g., hydrology signals not described by the deterministic model are present  
382 in the residuals fed into CMC). Under the realistic assumption that a component of the high frequency  
383 signal contained in CMC reflects real hydrological processes, we remove the contribution of surface  
384 hydrology using Global Land Data Assimilation System (GLDAS) (Rodell et al., 2004) VLD predictions.  
385 GLDAS does not model deep groundwater and open surface water, so these signals remain in the residual  
386 (Scanlon et al., 2018). VLD predictions driven by surface hydrology are derived similar to GRACE(-FO)  
387 (Section 2.2). We use Noah v2.1 monthly estimates of soil moisture storage given at 0.25-degree grids  
388 (Beaudoing and Rodell, 2016), convert the fields from terrestrial water storage ( $\text{kg}/\text{m}^2$ ) to units of  
389 equivalent water height, and predict the elastic response of the Earth (Eq. 1). Finally, we remove the  
390 reference epoch (09/2012) similar to GPS VLDs and derive the residuals relative to the deterministic  
391 model (Eq. 2). GLDAS (surface hydrology) residuals should ideally reflect high frequency hydrological  
392 processes and are therefore removed from GPS residuals. Overall, CMC of surface hydrology residuals  
393 exhibits a fairly small magnitude ( $\sim 0.5$  mm). We remove the contribution of surface hydrology within the  
394 CMC algorithm by first subtracting GLDAS VLD predictions from GPS, and next inputting the residuals  
395 of this difference into the algorithm. The output of this process ( $\text{CMC}_{\text{HF}}$ ) slightly decreases the magnitude  
396 of CMC and expresses a more realistic representation of spatially correlated noise.  
397

### 398 3.2 Results

399



400 VLD uncertainty of each station is estimated by means of all the different approaches discussed in Section  
401 3. The mean value and standard deviation are shown in Table 1. On average, an assumption of white  
402 noise shows slightly reduced uncertainty compared to the other techniques, followed by RMSE. When  
403 flicker noise is considered in addition to white noise (WN+FN) the average uncertainty increases by  
404 nearly 0.8 mm compared to the white noise only. Noise level from combination of all three noise models  
405 (WN+FN+RW) is somewhat less than 4 mm on average. CMC noise floor is 3.6 mm on average with a  
406 relatively large standard deviation ( $\pm 1.6$  mm) which suggests that spatially correlated noise has higher  
407 variability than time-correlated noise ( $\pm 1.6$  mm as opposed to  $\sim \pm 1$  mm). When surface hydrology is  
408 removed (CMC<sub>HF</sub>) the noise floor drops by a fraction of a mm on average compared to CMC.

409  
410 Table 1: Different uncertainty quantification cases

	$\mu$ (mm)	median (mm)	$\pm$ std (mm)
RMSE	2.8	2.7	0.8
WN	2.4	2.2	0.8
WN+FN	3.2	3.1	0.7
WN+FN+RW	3.8	3.5	1.1
CMC	3.6	3.2	1.6
CMC <sub>HF</sub>	3.5	3.1	1.6

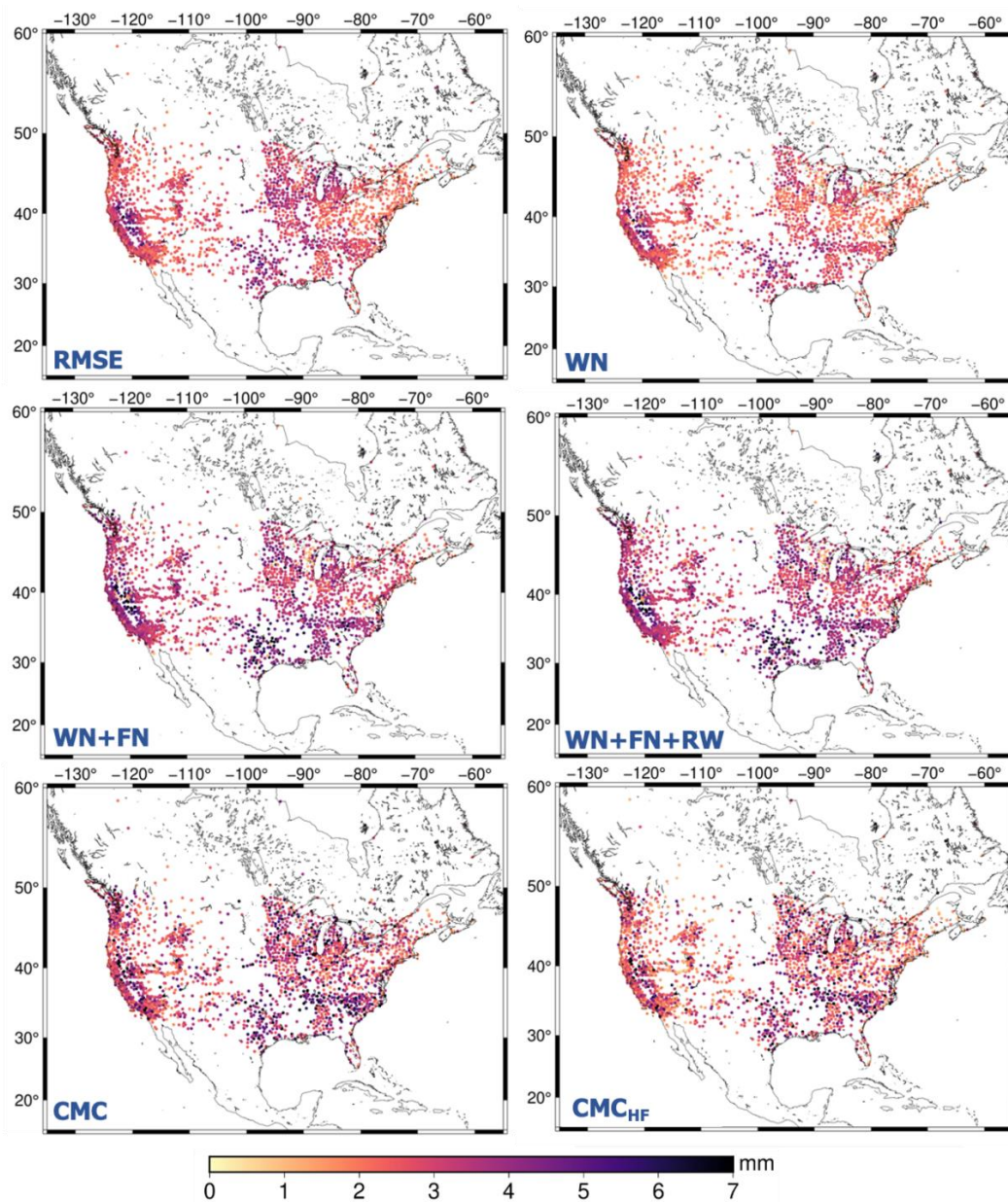
411  
412 RMSE and WN exhibit a smooth transition among the regions, which indicates the presence of spatially  
413 coherent regime signal mostly driven by hydrology (Fig. 6). The combination of WN+FN is mostly  
414 dominated by FN and the uncertainty exhibits local (in space) coherence. The uncertainty is larger when  
415 random walk is included in the combination (WN+FN+RW). A recent study from Argus et al. (2022) on  
416 groundwater flux in Central Valley (California) suggests that noise on GPS-derived uplift motion can be  
417 well described by a combination of flicker noise and random walk, due to the ability of these noise  
418 models to reflect low frequency noise. When a simulated contribution of the surface hydrological  
419 component is removed from the series, CMC<sub>HF</sub> reflects a more realistic picture of the noise. Arguably the  
420 level of change compared to CMC is sub-millimeter. Signal contributions from un-modelled groundwater  
421 variations are potentially still present, but groundwater changes are typically slower in time.

422  
423 We obtain the relative likelihood of each uncertainty quantification method by estimating the probability  
424 density function (PDF) (Fig. 7). White noise has a flat power spectrum, having the same amplitude  
425 across frequencies. Estimating a best fit for a flat spectrum doesn't allow for capturing the long tail skew  
426 of the residuals (low frequency), which are biased towards their mean. Thus, the amplitude of white noise  
427 is smaller compared to the rest of the techniques (Table 1). Flicker and random walk noise models add to  
428 the long tail of the power distribution, that is they allow more low frequency noise, which explains the  
429 higher amplitude of the uncertainty when these two noise types are considered.

430 RMSE and WN show a 50% probability of a station having an uncertainty ( $\sigma$ ) between 1.5-2 mm and less  
431 than 10% of a station exceeding  $\sigma=4$  mm. The noise level falls within [2 4] mm for  $\sim 93\%$  of the stations  
432 when we consider combination of WN+FN. PDF of RMSE, WN and WN+FN resemble a normal  
433 distribution, with the mean being shifted for each case. When random walk is also considered  
434 (WN+FN+RW) 64% of the stations exhibit noise within [2 4] mm. In this case, the distribution is more  
435 spread resembling a gamma-like distribution, with a peak being at 3 mm (18%). CMC and CMC<sub>HF</sub> PDF



436 also follow a gamma-shape, and the probability of the uncertainty ranging between [2 4] mm is nearly  
437 60% for CMC and 65% when surface hydrology is removed.  
438



439  
440 Figure 6: Uncertainty of GPS sites estimated using various techniques

441

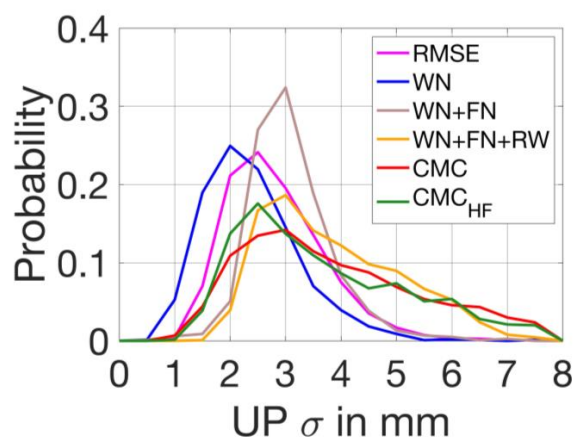


Figure 7: Probability density function of VLD estimates uncertainty

442  
443

444

#### 4. Discussion

445  
446

447 GPS VLD observations are very useful to supplement GRACE(-FO) gravity products to infer mass  
448 change signals at spatial scales smaller than what can typically be achieved with current satellite  
449 gravimetry alone (i.e., < 300km). This work provides a general workflow on isolating surface mass  
450 signals, developing processing standards and uncertainty quantification schemes of GPS VLD estimates,  
451 with the ultimate goal of merging them with satellite-gravimetry observations. First, we provide a list of  
452 corrections needed for isolating surface mass following recommendations outlined in Argus et al. (2017;  
453 2022). Additionally, detailed investigation of trends, correlation, and variance reduction, accentuates the  
454 need for better background modeling (GIA and interseismic strain), as the two observation platforms  
455 respond differently in the presence of such errors. At this point the recommendation is to remove sites  
456 located in the vicinity of regions where background models are known to perform poorly, before any joint  
457 inversion. Except detecting outlier stations, screening metrics point to extra corrections that need to be  
458 applied in certain sites (e.g., missed antenna offset in sites located in Michigan).  
459 Several uncertainty quantification schemes have been tested to prescribe weights on GPS VLD estimates  
460 for the joint inversion. The noise level is centered at 2 and 2.5 mm when uncertainty is derived as the  
461 RMSE of residuals or as white noise, respectively. Error increases when lower frequencies are included in  
462 the noise estimation. When we account for flicker noise, one third of the sites exhibits noise levels of up  
463 to 3 mm. The average noise increases significantly in presence of random walk, as more power of the  
464 lower frequencies gets into the estimations, and the distribution of noise is more dispersed. In this case,  
465 half of the stations are prescribed with > 4 mm uncertainty. Argus et al. (2022), suggests that random  
466 walk is the most realistic representation of noise based on postfit residuals. We notice that the spectrum of  
467 CMC provides similar uncertainties to random walk, which implies that despite the different  
468 characterization procedure, CMC is able to provide equally realistic noise estimates of GPS VLD  
469 timeseries. We strived to minimize lingering hydrology signals embedded in CMC, through reducing the  
470 GPS VLD observations with VLD from the GLDAS hydrology model. The average noise floor dropped  
471 slightly (~0.5 mm drop in sigma). Future work will potentially provide further information of GPS station  
472 errors when the weight of each GPS site is also considered based on its impact on the performance in a





473 formal data combination of GPS-GRACE(-FO). The suggested framework can be easily adjusted to  
474 account for global data sets. The new data set provides GPS vertical displacements of elastic mass  
475 variations in North America and their uncertainties.

476

477 **Data Availability:** The data product described in the manuscript is available in zenodo (doi:  
478 10.5281/zenodo.8184285). GPS timeseries are provided by the Global Station List from the Nevada  
479 Geodetic Laboratory (<http://geodesy.unr.edu/>; Blewitt et al., 2018). Non atmospheric and oceanic tidal  
480 aliasing product (AOD1B RL06) is provided by GFZ's Information System and Data Center  
481 (<ftp://isdc.gfz-potsdam.de/grace/Level-1B/GFZ/AOD/RL06>, Dobslaw et al., 2017). GRACE and  
482 GRACE-FO Level 2 products are available from podaac (<https://doi.org/10.5067/GFL20-MJ060>).  
483

484 **Acknowledgments:** The research was carried out at the Jet Propulsion Laboratory, California Institute  
485 of Technology, under a contract with the National Aeronautics and Space Administration  
486 (80NM0018D0004). Maps were made with the Generic Mapping Toolbox (Wessel et al. 2019).  
487

## 488 References

489

490 Akaike, H.: A new look at the statistical model identification. IEEE transactions on automatic control,  
491 19(6), pp.716-723. <https://doi.org/10.1109/TAC.1974.1100705>, 1974.

492

493 Altamimi, Z., Rebischung, P., Métivier, L. and Collilieux, X.: ITRF2014: A new release of the  
494 International Terrestrial Reference Frame modeling nonlinear station motions. Journal of Geophysical  
495 Research: Solid Earth, 121(8), pp.6109-6131. <https://doi.org/10.1002/2016JB013098>, 2016.

496

497 Amiri-Simkooei, A.R., Mohammadloo, T.H. and Argus, D.F.: Multivariate analysis of GPS position time  
498 series of JPL second reprocessing campaign. Journal of Geodesy, 91, pp.685-704.  
499 <https://doi.org/10.1007/s00190-016-0991-9>, 2017.

500

501 Argus, D.F., Fu, Y. and Landerer, F.W.: Seasonal variation in total water storage in California inferred  
502 from GPS observations of vertical land motion. Geophysical Research Letters, 41(6), pp.1971-1980.  
503 <https://doi.org/10.1002/2014GL059570>, 2014.

504

505 Argus, D.F., Gordon, R.G., Heflin, M.B., Ma, C., Eanes, R.J., Willis, P., Peltier, W.R. and Owen, S.E.:  
506 The angular velocities of the plates and the velocity of Earth's centre from space geodesy. Geophysical  
507 Journal International, 180(3), pp.913-960. <https://doi.org/10.1111/j.1365-246X.2009.04463.x>, 2010.

508

509 Argus, D.F., Landerer, F.W., Wiese, D.N., Martens, H.R., Fu, Y., Famiglietti, J.S., Thomas, B.F., Farr,  
510 T.G., Moore, A.W. and Watkins, M.M.: Sustained water loss in California's mountain ranges during  
511 severe drought from 2012 to 2015 inferred from GPS. Journal of Geophysical Research: Solid Earth,  
512 122(12), pp.10-559. <https://doi.org/10.1002/2017JB014424>, 2017.

513

514 Argus, D.F., Martens, H.R., Borsa, A.A., Knappe, E., Wiese, D.N., Alam, S., Anderson, M., Khatiwada,  
515 A., Lau, N., Peidou, A. and Swarr, M.: Subsurface water flux in California's Central Valley and its source  
516 watershed from space geodesy. Geophysical Research Letters, 49(22), p.e2022GL099583.  
517 <https://doi.org/10.1029/2022GL099583>, 2022.

518

519 Argus, D.F., Peltier, W.R., Blewitt, G. and Kreemer, C.: The Viscosity of the Top Third of the Lower  
520 Mantle Estimated Using GPS, GRACE, and Relative Sea Level Measurements of Glacial Isostatic



- 521 Adjustment. *Journal of Geophysical Research: Solid Earth*, 126(5), p.e2020JB021537.  
522 <https://doi.org/10.1029/2020JB021537>, 2021.  
523  
524 Beaudoin, H. and M. Rodell: GLDAS Noah Land Surface Model L4 monthly 0.25 x 0.25 degree V2.1,  
525 Greenbelt, Maryland, USA, Goddard Earth Sciences Data and Information Services Center (GES DISC).  
526 <https://doi.org/10.5067/SXAVCZFAQLNO>, 2020.  
527  
528 Becker, J.M. and Bevis, M.: Love's problem. *Geophysical Journal International*, 156(2), pp.171-178.  
529 <https://doi.org/10.1111/j.1365-246X.2003.02150.x>, 2004.  
530  
531 Bertiger, W., Bar-Sever, Y., Dorsey, A., Haines, B., Harvey, N., Hemberger, D., Heflin, M., Lu, W.,  
532 Miller, M., Moore, A.W. and Murphy, D.: GipsyX/RTGx, a new tool set for space geodetic operations  
533 and research. *Advances in space research*, 66(3), pp.469-489. <https://doi.org/10.1016/j.asr.2020.04.015>,  
534 2020.  
535  
536 Blewitt, G., Hammond, W.C. and Kreemer, C., 2018. Harnessing the GPS data explosion for  
537 interdisciplinary science. *Eos*, 99(10.1029), p.485. doi.org/10.1029/2018EO104623.  
538 <https://doi.org/10.1029/2018EO104623>,  
539  
540 Blewitt, G., Lavallée, D., Clarke, P. and Nurutdinov, K.: A new global mode of Earth deformation:  
541 Seasonal cycle detected. *Science*, 294(5550), pp.2342-2345.  
542 <https://doi.org/10.1126/science.1065328>, 2001.  
543  
544 Borsa, A.A., Agnew, D.C. and Cayan, D.R.: December. Drought-induced uplift in the western United  
545 States as observed by the EarthScope Plate Boundary Observatory GPS network. In AGU Fall Meeting  
546 Abstracts (Vol. 2014, pp. G23B-0481), 2014.  
547  
548 Bos, M.S., Fernandes, R.M.S., Williams, S.D.P. and Bastos, L.: Fast error analysis of continuous GPS  
549 observations. *Journal of Geodesy*, 82(3), pp.157-166. <https://doi.org/10.1007/s00190-007-0165-x>, 2008.  
550  
551 Bos, M.S., Fernandes, R.M.S., Williams, S.D.P. and Bastos, L.: Fast error analysis of continuous GPS  
552 observations with missing data. *Journal of Geodesy*, 87(4), pp.351-360. <https://doi.org/10.1007/s00190-012-0605-0>, 2013.  
553  
554  
555 Chew, C.C. and Small, E.E.: Terrestrial water storage response to the 2012 drought estimated from GPS  
556 vertical position anomalies. *Geophysical Research Letters*, 41(17), pp.6145-6151.  
557 <https://doi.org/10.1002/2014GL061206>, 2014.  
558  
559 Crowell, B.W., Bock, Y. and Liu, Z.: Single-station automated detection of transient deformation in GPS  
560 time series with the relative strength index: A case study of Cascadian slow slip. *Journal of Geophysical*  
561 *Research: Solid Earth*, 121(12), pp.9077-9094. <https://doi.org/10.1002/2016JB013542>, 2016.  
562  
563 Davis, J.L., Elósegui, P., Mitrovica, J.X. and Tamisiea, M.E.: Climate-driven deformation of the solid  
564 Earth from GRACE and GPS. *Geophysical Research Letters*, 31(24).  
565 <https://doi.org/10.1029/2004GL021435>, 2004.  
566  
567 Dee, D.P., Uppala, S.M., Simmons, A.J., Berrisford, P., Poli, P., Kobayashi, S., Andrae, U., Balmaseda,  
568 M.A., Balsamo, G., Bauer, D.P. and Bechtold, P.: The ERA-Interim reanalysis: Configuration and  
569 performance of the data assimilation system. *Quarterly Journal of the royal meteorological society*,  
570 137(656), pp.553-597. <https://doi.org/10.1002/qj.828>, 2011.  
571



- 572 Dobslaw, H., Bergmann-Wolf, I., Dill, R., Poropat, L., Thomas, M., Dahle, C., Esselborn, S., König, R.  
573 and Flechtner, F.: A new high-resolution model of non-tidal atmosphere and ocean mass variability for  
574 de-aliasing of satellite gravity observations: AOD1B RL06. *Geophysical Journal International*, 211(1),  
575 pp.263-269. <https://doi.org/10.1093/gji/ggx302>, 2017.  
576
- 577 Frederikse, T., Landerer, F., Caron, L., Adhikari, S., Parkes, D., Humphrey, V.W., Dangendorf, S.,  
578 Hogarth, P., Zanna, L., Cheng, L. and Wu, Y.H.: The causes of sea-level rise since 1900. *Nature*,  
579 584(7821), pp.393-397. <https://doi.org/10.1038/s41586-020-2591-3>, 2020.  
580
- 581 Fu, Y. and Freymueller, J.T.: Seasonal and long-term vertical deformation in the Nepal Himalaya  
582 constrained by GPS and GRACE measurements. *Journal of Geophysical Research: Solid Earth*, 117(B3).  
583 <https://doi.org/10.1029/2011JB008925>, 2012.  
584
- 585 Fu, Y., Argus, D.F. and Landerer, F.W.: GPS as an independent measurement to estimate terrestrial water  
586 storage variations in Washington and Oregon. *Journal of Geophysical Research: Solid Earth*, 120(1),  
587 pp.552-566. <https://doi.org/10.1002/2014JB011415>, 2015.  
588
- 589 Fukumori, I., Wang, O., Llovel, W., Fenty, I. and Forget, G.: A near-uniform fluctuation of ocean bottom  
590 pressure and sea level across the deep ocean basins of the Arctic Ocean and the Nordic Seas. *Progress in*  
591 *Oceanography*, 134, pp.152-172. <https://doi.org/10.1016/j.pocean.2015.01.013>, 2015.  
592
- 593 Gazeaux, J., Williams, S., King, M., Bos, M., Dach, R., Deo, M., Moore, A.W., Ostini, L., Petrie, E.,  
594 Roggero, M. and Teferle, F.N.: Detecting offsets in GPS time series: First results from the detection of  
595 offsets in GPS experiment. *Journal of Geophysical Research: Solid Earth*, 118(5), pp.2397-2407.  
596 <https://doi.org/10.1002/jgrb.50152>, 2013.  
597
- 598 He, X., Bos, M.S., Montillet, J.P. and Fernandes, R.M.S.: Investigation of the noise properties at low  
599 frequencies in long GPS time series. *Journal of Geodesy*, 93(9), pp.1271-1282.  
600 <https://doi.org/10.1007/s00190-019-01244-y>, 2019.  
601
- 602 Houborg, R., Rodell, M., Li, B., Reichle, R. and Zaitchik, B.F.: Drought indicators based on model-  
603 assimilated Gravity Recovery and Climate Experiment (GRACE) terrestrial water storage observations.  
604 *Water Resources Research*, 48(7). <https://doi.org/10.1029/2011WR011291>, 2012.  
605
- 606 Ji, K.H. and Herring, T.A. A method for detecting transient signals in GPS position time-series:  
607 smoothing and principal component analysis. *Geophysical Journal International*, 193(1), pp.171-186.  
608 <https://doi.org/10.1093/gji/ggt003>, 2013.  
609
- 610 Jiang, W., Li, Z., van Dam, T. and Ding, W.: Comparative analysis of different environmental loading  
611 methods and their impacts on the GPS height time series. *Journal of Geodesy*, 87(7), pp.687-703.  
612 <https://doi.org/10.1007/s00190-013-0642-3>, 2013.  
613
- 614 Klos, A., Bogusz, J., Figurski, M. and Kosek, W.: Uncertainties of geodetic velocities from permanent  
615 GPS observations: the Sudeten case study. *Acta Geodynamica et Geomaterialia*, 11(3), p.175.  
616 <https://doi.org/10.13168/AGG.2014.0005>, 2014.  
617
- 618 Klos, A., Dobslaw, H., Dill, R. and Bogusz, J.: Identifying the sensitivity of GPS to non-tidal loadings at  
619 various time resolutions: examining vertical displacements from continental Eurasia. *GPS Solutions*,  
620 25(3), p.89. <https://doi.org/10.1007/s10291-021-01135-w>, 2021.  
621



- 622 Klos, A., Kusche, J., Fenoglio-Marc, L., Bos, M.S. and Bogusz, J.: Introducing a vertical land  
623 displacement model for improving estimates of sea level rates derived from tide gauge records affected by  
624 earthquakes. *GPS Solutions*, 23(4), pp.1-12. <https://doi.org/10.1007/s10291-019-0896-1>, 2019.
- 625  
626 Kreemer, C. and Blewitt, G.: Robust estimation of spatially varying common-mode components in GPS  
627 time-series. *Journal of geodesy*, 95(1), pp.1-19. <https://doi.org/10.1007/s00190-020-01466-5>, 2021.
- 628  
629 Kumar, U., Chao, B.F. and Chang, E.T.: What causes the common-mode error in array GPS displacement  
630 fields: Case study for Taiwan in relation to atmospheric mass loading. *Earth and Space Science*, 7(11),  
631 p.e2020EA001159. <https://doi.org/10.1029/2020EA001159>, 2020.
- 632  
633 Landerer, F.W., Flechtner, F.M., Save, H., Webb, F.H., Bandikova, T., Bertiger, W.I., Bettadpur, S.V.,  
634 Byun, S.H., Dahle, C., Dobslaw, H. and Fahnestock, E.: Extending the global mass change data record:  
635 GRACE Follow-On instrument and science data performance. *Geophysical Research Letters*, 47(12),  
636 p.e2020GL088306. <https://doi.org/10.1029/2020GL088306>, 2020.
- 637  
638 Li, S., Wang, K., Wang, Y., Jiang, Y. and Dosso, S.E.: Geodetically inferred locking state of the Cascadia  
639 megathrust based on a viscoelastic Earth model. *Journal of Geophysical Research: Solid Earth*, 123(9),  
640 pp.8056-8072. <https://doi.org/10.1029/2018JB015620>, 2018.
- 641  
642 Li, W. and Shen, Y.: The consideration of formal errors in spatiotemporal filtering using principal  
643 component analysis for regional GPS position time series. *Remote Sensing*, 10(4), p.534.  
644 <https://doi.org/10.3390/rs10040534>, 2018.
- 645  
646 Liu, B., Dai, W., Peng, W. and Meng, X.: Spatiotemporal analysis of GPS time series in vertical direction  
647 using independent component analysis. *Earth, Planets and Space*, 67(1), pp.1-10.  
648 <https://doi.org/10.1186/s40623-015-0357-1>, 2015.
- 649  
650 Loomis, B.D., Rachlin, K.E. and Luthcke, S.B.: Improved Earth oblateness rate reveals increased ice  
651 sheet losses and mass-driven sea level rise. *Geophysical Research Letters*, 46(12), pp.6910-6917.  
652 <https://doi.org/10.1029/2019GL082929>, 2019.
- 653  
654 Michel, A., Santamaría-Gómez, A., Boy, J.P., Perosanz, F. and Loyer, S.: Analysis of GPS Displacements  
655 in Europe and Their Comparison with Hydrological Loading Models. *Remote Sensing*, 13(22), p.4523.  
656 <https://doi.org/10.3390/rs13224523>, 2021.
- 657  
658 Milliner, C., Materna, K., Bürgmann, R., Fu, Y., Moore, A.W., Bekaert, D., Adhikari, S. and Argus, D.F.:  
659 Tracking the weight of Hurricane Harvey's stormwater using GPS data. *Science advances*, 4(9),  
660 p.eaau2477. <https://doi.org/10.1126/sciadv.aau2477>, 2018.
- 661  
662 Montillet, J.P., Melbourne, T.I. and Szeliga, W.M.: GPS vertical land displacement corrections to sea-  
663 level rise estimates in the Pacific Northwest. *Journal of Geophysical Research: Oceans*, 123(2), pp.1196-  
664 1212. <https://doi.org/10.1002/2017JC013257>, 2018.
- 665  
666 Nikolaidis, R.: Observation of geodetic and seismic deformation with the Global Positioning System.  
667 University of California, San Diego, 2002.
- 668  
669 Pail, R., Bingham, R., Braitenberg, C., Dobslaw, H., Eicker, A., Güntner, A., Horwath, M., Ivins, E.,  
670 Longueuevigne, L., Panet, I. and Wouters, B.: Science and user needs for observing global mass transport  
671 to understand global change and to benefit society. *Surveys in Geophysics*, 36(6), pp.743-772.  
672 <https://doi.org/10.1007/s10712-015-9348-9>, 2015.



- 673  
674 Peltier, W. R., Argus, D. F., and Drummond, R.: Comment on the paper by Purcell et al. 2016 entitled 'An  
675 assessment of ICE-6G\_C (VM5a) glacial isostatic adjustment model (2018). *Journal Geophysical*  
676 *Research: Solid Earth*, 122, 2019-2028. <https://doi.org/10.1002/2016JB013844>, 2018.  
677  
678 Ray, J., Altamimi, Z., Collilieux, X. and van Dam, T.: Anomalous harmonics in the spectra of GPS  
679 position estimates. *GPS solutions*, 12, pp.55-64. <https://doi.org/10.1007/s10291-007-0067-7>, 2008.  
680  
681 Reager, J.T., Thomas, B.F. and Famiglietti, J.S.: River basin flood potential inferred using GRACE  
682 gravity observations at several months lead time. *Nature Geoscience*, 7(8), pp.588-592.  
683 <https://doi.org/10.1038/ngeo2203>, 2014.  
684  
685 Rodell, M., Houser, P.R., Jambor, U.E.A., Gottschalck, J., Mitchell, K., Meng, C.J., Arsenault, K.,  
686 Cosgrove, B., Radakovich, J., Bosilovich, M. and Entin, J.K.: The global land data assimilation system.  
687 *Bulletin of the American Meteorological society*, 85(3), pp.381-394.  
688 <https://doi.org/10.1175/BAMS-85-3-381>, 2004.  
689  
690 Rodriguez-Solano, C.J., Hugentobler, U., Steigenberger, P., Bloßfeld, M. and Fritsche, M.: Reducing the  
691 draconitic errors in GPS geodetic products. *Journal of Geodesy*, 88(6), pp.559-574.  
692 <https://doi.org/10.1007/s00190-014-0704-1>, 2014.  
693  
694 Rui, H., Beaudoin, H. and Loeser, C.: README document for NASA GLDAS version 2 data products.  
695 Goddard Earth Sciences Data and Information Services Center (GES DISC): Greenbelt, MD, USA, 2018.  
696  
697 Santamaria-Gomez, A., Gravelle, M., Collilieux, X., Guichard, M., Míguez, B.M., Tiphaneau, P. and  
698 Wöppelmann, G.: Mitigating the effects of vertical land displacement in tide gauge records using a state-  
699 of-the-art GPS velocity field. *Global and Planetary Change*, 98, pp.6-17.  
700 <https://doi.org/10.1016/j.gloplacha.2012.07.007>, 2012.  
701  
702 Schwarz, G.: Estimating the dimension of a model. *Annals of statistics*, 6(2), pp.461-464.  
703 <https://doi.org/10.1214/aos/1176344136>, 1978.  
704  
705 Serpelloni, E., Faccenna, C., Spada, G., Dong, D. and Williams, S.D.: Vertical GPS ground motion rates  
706 in the Euro-Mediterranean region: New evidence of velocity gradients at different spatial scales along the  
707 Nubia-Eurasia plate boundary. *Journal of Geophysical Research: Solid Earth*, 118(11), pp.6003-6024.  
708 <https://doi.org/10.1002/2013JB010102>, 2013.  
709  
710 Simmons, A., Uppala, S., Dee, D. and Kobayashi, S.: ERA-Interim: New ECMWF reanalysis products  
711 from 1989 onwards. *ECMWF newsletter*, 110, 25-35. <https://doi.org/10.21957/pocnex23c6>, 2007.  
712  
713 Sun, Y., Riva, R. and Ditmar, P.: Optimizing estimates of annual variations and trends in geocenter  
714 motion and J2 from a combination of GRACE data and geophysical models, *J. Geophys. Res. Solid Earth*,  
715 121, <https://doi.org/10.1002/2016JB013073>, 2016.  
716  
717 Tapley, B.D., Watkins, M.M., Flechtner, F., Reigber, C., Bettadpur, S., Rodell, M., Sasgen, I.,  
718 Famiglietti, J.S., Landerer, F.W., Chambers, D.P. and Reager, J.T.: Contributions of GRACE to  
719 understanding climate change. *Nature climate change*, 9(5), pp.358-369.  
720 <https://doi.org/10.1038/s41558-019-0456-2>, 2019.  
721



- 722 Thomas, A.C., Reager, J.T., Famiglietti, J.S. and Rodell, M.: A GRACE-based water storage deficit  
723 approach for hydrological drought characterization. *Geophysical Research Letters*, 41(5), pp.1537-1545.  
724 <https://doi.org/10.1002/2014GL059323>, 2014.
- 725  
726 Thomas, B.F., Famiglietti, J.S., Landerer, F.W., Wiese, D.N., Molotch, N.P. and Argus, D.F.:  
727 Groundwater drought index: Evaluation of California Central Valley groundwater drought. *Remote*  
728 *Sensing of Environment*, 198, pp.384-392. <https://doi.org/10.1016/j.rse.2017.06.026>, 2017.
- 729  
730 Tian, Y. and Shen, Z.K.: Extracting the regional common-mode component of GPS station position time  
731 series from dense continuous network. *Journal of Geophysical Research: Solid Earth*, 121(2), pp.1080-  
732 1096. <https://doi.org/10.1002/2015JB012253>, 2016.
- 733  
734 Tregoning, P., Watson, C., Ramillien, G., McQueen, H. and Zhang, J.: Detecting hydrologic deformation  
735 using GRACE and GPS. *Geophysical Research Letters*, 36(15). <https://doi.org/10.1029/2009GL038718>,  
736 2009.
- 737  
738 Tsai, V.C.: A model for seasonal changes in GPS positions and seismic wave speeds due to thermoelastic  
739 and hydrologic variations. *Journal of Geophysical Research: Solid Earth*, 116(B4).  
740 <https://doi.org/10.1029/2010JB008156>, 2011.
- 741  
742 van Dam, T., Wahr, J. and Lavallée, D.: A comparison of annual vertical crustal displacements from GPS  
743 and Gravity Recovery and Climate Experiment (GRACE) over Europe. *Journal of Geophysical Research:*  
744 *Solid Earth*, 112(B3). <https://doi.org/10.1029/2006JB004335>, 2007.
- 745  
746 Van Dam, T., Wahr, J., Milly, P.C.D., Shmakin, A.B., Blewitt, G., Lavallée, D. and Larson, K.M.: Crustal  
747 displacements due to continental water loading. *Geophysical Research Letters*, 28(4), pp.651-654.  
748 <https://doi.org/10.1029/2000GL012120>, 2001.
- 749  
750 Velicogna, I., Mohajerani, Y., Landerer, F., Mouginit, J., Noel, B., Rignot, E., Sutterley, T., van den  
751 Broeke, M., van Wessem, M. and Wiese, D.: Continuity of ice sheet mass loss in Greenland and  
752 Antarctica from the GRACE and GRACE Follow-On missions. *Geophysical Research Letters*, 47(8),  
753 p.e2020GL087291. <https://doi.org/10.1029/2020GL087291>, 2020.
- 754  
755 Wang, H., Xiang, L., Jia, L., Jiang, L., Wang, Z., Hu, B. and Gao, P.: Load Love numbers and Green's  
756 functions for elastic Earth models PREM, iasp91, ak135, and modified models with refined crustal  
757 structure from Crust 2.0. *Computers & Geosciences*, 49, pp.190-199.  
758 <https://doi.org/10.1016/j.cageo.2012.06.022>, 2012.
- 759  
760 Watkins, M.M., Wiese, D.N., Yuan, D.N., Boening, C. and Landerer, F.W.: Improved methods for  
761 observing Earth's time variable mass distribution with GRACE using spherical cap mascons. *Journal of*  
762 *Geophysical Research: Solid Earth*, 120(4), pp.2648-2671. <https://doi.org/10.1002/2014JB011547>, 2015.
- 763  
764 Wdowinski, S., Bock, Y., Zhang, J., Fang, P. and Genrich, J.: Southern California permanent GPS  
765 geodetic array: Spatial filtering of daily positions for estimating coseismic and postseismic displacements  
766 induced by the 1992 Landers earthquake. *Journal of Geophysical Research: Solid Earth*, 102(B8),  
767 pp.18057-18070. <https://doi.org/10.1029/97JB01378>, 1997.
- 768  
769 Wessel, P., Luis, J.F., Uieda, L., Scharroo, R., Wobbe, F., Smith, W.H. and Tian, D.: The generic  
770 mapping tools version 6. *Geochemistry, Geophysics, Geosystems*, 20(11), pp.5556-5564.  
771 <https://doi.org/10.1029/2019GC008515>, 2019.
- 772



- 773 Wiese, D.N., Bienstock, B., Blackwood, C., Chrono, J., Loomis, B.D., Sauber, J., Rodell, M., Baize, R.,  
774 Bearden, D., Case, K. and Horner, S.: The mass change designated observable study: overview and  
775 results. *Earth and Space Science*, 9(8), p.e2022EA002311. <https://doi.org/10.1029/2022EA002311>, 2022.  
776
- 777 Wiese, D.N., Landerer, F.W. and Watkins, M.M.: Quantifying and reducing leakage errors in the JPL  
778 RL05M GRACE mascon solution. *Water Resources Research*, 52(9), pp.7490-7502.  
779 <https://doi.org/10.1002/2016WR019344>, 2016.  
780
- 781 Williams, S.D.: CATS: GPS coordinate time series analysis software. *GPS solutions*, 12(2), pp.147-153.  
782 <https://doi.org/10.1007/s10291-007-0086-4>, 2008.  
783
- 784 Williams, S.D., Bock, Y., Fang, P., Jamason, P., Nikolaidis, R.M., Prawirodirdjo, L., Miller, M. and  
785 Johnson, D.J.: Error analysis of continuous GPS position time series. *Journal of Geophysical Research:*  
786 *Solid Earth*, 109(B3). <https://doi.org/10.1029/2003JB002741>, 2004.  
787
- 788 Wu, S., Nie, G., Liu, J., Wang, K., Xue, C., Wang, J., Li, H., Peng, F. and Ren, X.: A sub-regional  
789 extraction method of common mode components from IGS and CMONOC stations in China. *Remote*  
790 *Sensing*, 11(11), p.1389. <https://doi.org/10.3390/rs11111389>, 2019.  
791
- 792 Yin, G., Forman, B.A., Loomis, B.D. and Luthcke, S.B.: Comparison of Vertical Surface Deformation  
793 Estimates Derived From Space-Based Gravimetry, Ground-Based GPS, and Model-Based Hydrologic  
794 Loading Over Snow-Dominated Watersheds in the United States. *Journal of Geophysical Research: Solid*  
795 *Earth*, 125(8), p.e2020JB01943. <https://doi.org/10.1029/2020JB019432>, 2020.